We are IntechOpen, the world's leading publisher of Open Access books
Built by scientists, for scientists

6,900
Open access books available

185,000
International authors and editors

200M
Downloads

154
Countries delivered to

Our authors are among the

TOP 1%
most cited scientists

12.2%
Contributors from top 500 universities

BOOK CITATION INDEX
CLARIVATE ANALYTICS
INDEXED

WEB OF SCIENCE™

Selection of our books indexed in the Book Citation Index
in Web of Science™ Core Collection (BKCI)

Interested in publishing with us?
Contact book.department@intechopen.com

Application of Optical CT Scanning in Three-Dimensional Radiation Dosimetry

Andy Y. Xu and C. S. Wuu
Department of Radiation Oncology, Columbia University
New York, NY,
USA

1. Introduction

There has been much research effort in the development of an accurate and reliable three-dimensional dose verification system, prompted by the advances of technologies in radiation treatment of cancer patients. New radiotherapy techniques such as intensity modulated radiation therapy (IMRT), stereotactic radiosurgery (SRS) and high dose rate (HDR) brachytherapy are aimed at dose deliveries that are highly localized within the tumor volumes. The dose distributions from these treatment methods are typically characterized with high dose gradients around the boundaries of the targets, which present certain challenges for one or two-dimensional dosimeters such as film, TLD, and ion chamber (Webb, 2001).

In recent years, gel dosimeter has emerged as a promising candidate for 3D dosimetry (Baldock et al, 2010). Extensive studies have been done on the development of different types of gel formulas (Maryanski et al, 1996; Baldock et al, 1998; Pappas et al, 1999; Fong et al, 2001; Adamovics and Maryanski, 2006). Between the two classes of gel dosimeters that have been studied so far, the radiochromic Fricke gel is easier to make and handle than the polymer gel, but it suffers from a major error of diffusion. The blurring of the dose distribution image within time as short as an hour makes it inconvenient to be implemented into clinics. The polymer gel has the advantage of preserving the spatial accuracy of the dose distribution, but is sensitive to oxygen contamination and thus needs to be made freshly before each measurement. Furthermore, both types of gels suffer from a long-term drift of the baseline optical density, either due to self-oxidation of the ferrous ions in the Fricke gel or polymerization initiated by the redox reactions in the polymer gel.

The readout of gel dosimeters was initially conducted by magnetic-resonance imaging (MRI) (Gore et al, 1984; Maryanski et al, 1993; Audet and Schreiner 1997; De Deene et al, 1998; Low et al, 1999; Lepage et al, 2002) and subsequently extended to other imaging modalities such as optical computed tomography (CT) (Gore et al, 1996; Kelly et al, 1998; Doran et al, 2001; Xu et al, 2003), X-ray CT (Hilts et al, 2000) and ultrasound (Mather and Baldock, 2003). The idea of optical CT was first introduced to gel dosimetry in 1996 (Gore et al, 1996) together with a new tissue equivalent polymer gel dosimeter (Maryanski et al, 1996). Since then, optical CT scanners in a variety of forms have been built for imaging gel phantoms irradiated with photon, electron, proton beams as well as brachytherapy radiation sources (Islam et al, 2003; Wuu et al, 2003; Oldham and Kim, 2004; Xu et al, 2004; Doran et al, 2006; DeJean et al, 2006;

Krstajic and Doran, 2006; Sakhalkar and Oldham, 2008; Olding et al, 2010). Currently, the advantage of the optical CT approach over other dose readout methods for gel dosimetry is commonly acknowledged (Oldham et al, 2001; Lopatiuk-Tirpak et al, 2008). It has been postulated that gel dosimetry using a bench-top optical CT scanner will be a valuable tool for patient specific treatment dose verification, periodic quality assurance of radiation therapy units, and commissioning of new treatment techniques and machines.

The purpose of this paper is to give a brief summary of the challenges that are unique in optical CT-based 3D radiation dosimetry. The structure of the chapter is as follows: section 2 describes the two classes of optical CT scanners that have been developed so far; section 3 addresses the use of refractive index matching liquid for minimizing the multiple reflection and refraction at the boundary of a dosimeter; section 4 discusses the dynamic range problem associated with three-dimensional optical CT; section 5 summaries the effects of light scattering on the reconstructed dose distribution in optical CT; section 6 gives the results from 3D dosimeters irradiated with three representative radiation treatment plans.

2. Speed and accuracy of optical CT scanning

When radiation is delivered to a gel phantom, the physical properties (density or color) of the gel material inside the phantom will change according to the dose distribution deposited. Optical computed tomography can be used to generate a three-dimensional optical density map to reproduce the recorded dose distribution. Optical CT is a technique analogous to x-ray CT, except utilizing visible light instead of x-rays. The designing of optical CT scanners for gel dosimetry has been driven by two major considerations. First, unlike X-ray CT, the reconstructed images from optical CT need to be quantitatively accurate to within a few percent. This imposes certain limitations on the implementation of the existing technologies from X-ray CT in gel dosimetry. Second, acquisition of a complete set of 3D images from a gel dosimeter should be done reasonably fast rendering the dosimetric verification system practical for routine clinical practice. As such, two groups of optical CT scanners have been built. One is based on a single laser source coupled to a single photodiode detector and the other uses an incoherent broad light source and a large area detector such as a CCD camera.
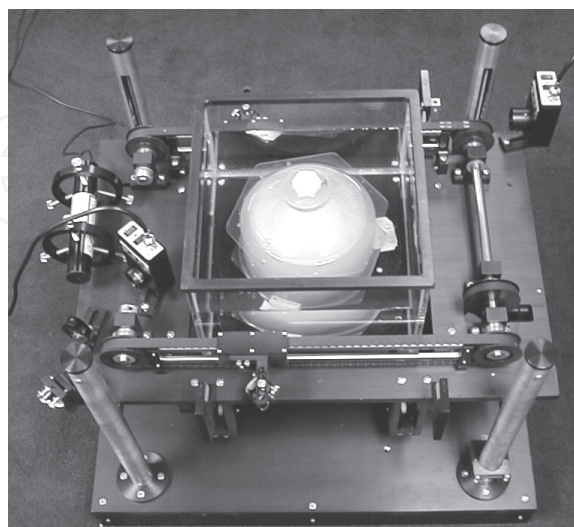

Fig. 1. Top view of the OCT-OPUS™ research scanner (MGS Research, Inc., Madison, CT, USA) with a Barex gel cylinder mounted in the scanning tank.

Figure 1 is a picture of the OCT-OPUS™ optical CT scanner (MGS Research, Inc., Madison, CT, USA) with a gel cylinder mounted for scanning. The basic running principle and the prototype configuration of this scanner can be summarized as the following (Gore et al, 1996; Xu et al, 2004). A single He-Ne laser beam (633-nm wavelength) is guided by a stepper motor and a series of mirrors and lenses to scan across a rectangular water tank repeatedly with a fixed field of view. The light transmitted through the tank is collected by a photodiode during each cycle of translational motions as single projection data. The laser output can be monitored by a reference photodiode through measurement of the light reflected from a beam-splitter. The photodiode voltage signals are fed into two different channels of a 16-bit plug-in PCI data acquisition board. The gel to be scanned is mounted on a turntable at the bottom of the scanner's tank. The tank is otherwise filled with a liquid mixture of water, glycerol and a blue dye, to minimize the effect of reflection and refraction around the container wall. The turntable rotates 360 degrees at a selected angular increment to collect projection data for a planar image.

Three dimensional CT scanning is realized based on the motion of 3 stepper motors. Motor #1 is mounted on the scanning platform to move the scanning mirror to generate parallel scanning laser beams. Motor #2 is connected to the turntable within the water tank to position the imaged dosimeters at different rotation angles. Motor #3 is used to drive the scanning platform up and down relative to the water tank for slice selection.

Data acquisition is synchronized with the motion of the scanning mirror. A pixel is defined as the distance traveled by the scanning mirror while 100 data points are sampled. The signal for each pixel is taken as the average of these 100 points. The data acquisition rate, the pixel size, the pixel numbers per projection and the number of projections per slice are controlled by the user. The whole process of scanning and data acquisition is controlled by a computer program written with TESTPOINT.

The unit-length optical density distribution for a transverse slice is reconstructed from the projection data using filtered back projection with the Shepp-Logan filter. The reconstructed images can be viewed and analyzed by the ImageJ software (http://rsb.info.nih.gov/ij) or imported into a computer program for isodose analysis in the transverse, coronal and sagittal directions.
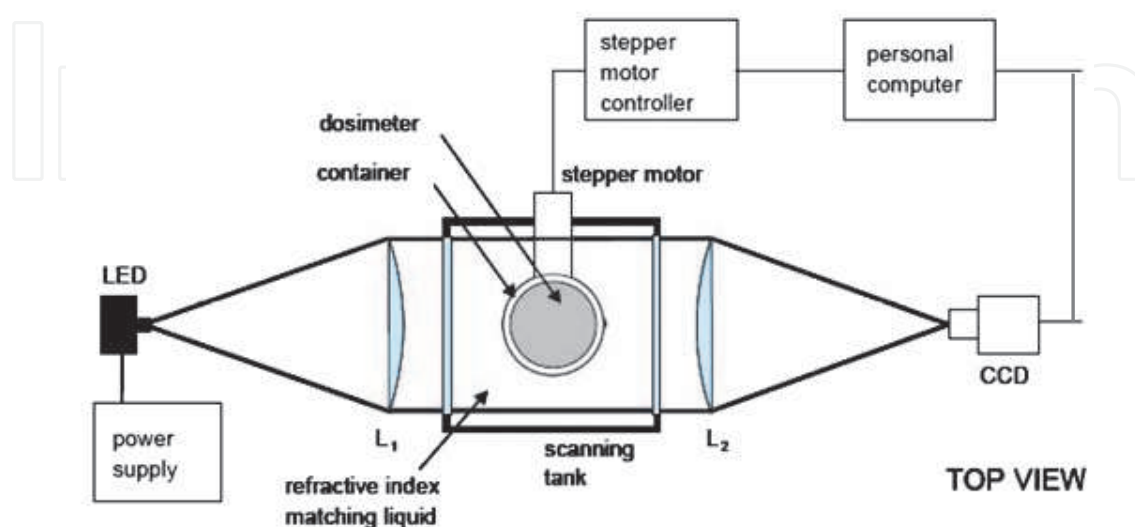

Fig. 2. Schematic diagram of a CCD-camera based optical tomography scanner.

Figure 2 is a schematic picture of an optical CT scanner using a broad, collimated beam and a charge coupled detector (CCD) (Krstajic and Doran, 2006). To summarize, a LED light source sits behind a circular pinhole of 1 mm diameter. The pinhole is placed on the focal point of collimating lens L1, creating a parallel beam. The parallel beam passes through the water tank and gets focused by lens L2 on to a CCD lens. The CCD lens focuses the incoming light rays further onto a CCD chip inside the camera. The scanned dosimeter is placed on a rotation stage driven by a stepper motor. The stepper motor rotates the dosimeter while the CCD takes images via a PC frame-grabber card in a 'stop and shoot' protocol. Data acquisition and rotation control are synchronized via an in-house develop computer program.

CCD-based optical CT scanners can also be designed using cone-beam configuration. This was first proposed by Wolodzko et al (1999) and a similar device is marketed as a research tool by Modus Medical devices Inc. (London, Ontario, Canada) under the name *Vista*.

Optical CT scanners using broad light sources are inherently fast. There is no technical difficulty in acquiring all the raw data points from an irradiated gel via a CCD camera within a few minutes. However, the use of broad light sources and large area detectors presents certain challenges for separating the useful signal from various other signal contributions. In particular, the deviation of the light rays from straight line passages caused by various inhomogeneities within the imaged objects will be difficult to model and ultimately limit the accuracy of the approach. This problem could be more severe than that in X-ray CT and megavoltage portal dosimetry considering the high penetrating power of the X-ray beams and the quantitative accuracy requirement from gel dosimetry.

The scanners using a point laser beam and a single photodiode detector do not suffer from the intrinsic light "entanglement" problem but have the limitation of long scanning time. For instance, it could take up to 10 hours for the first generation of the OCTOPUS™ scanner (MGS Research Inc., Madison, CT, USA) to perform a 3D scan on a dosimeter of regular size with 1 mm resolution in three dimensions. Therefore, the scanner has been used only for research purpose so far even though it is accurate and stable enough for clinical use.

Development of clinically applicable optical CT scanners has been moving in two directions: to increase the speed of the scanners using single laser sources; and to improve the accuracy of the scanners using broad beam illumination.

3. Refractive index matching liquid

In conventional x-ray CT, the refraction of the primary beam at the interface of different materials was never a concern because the refractive index of X-rays in most of media is close to one. So deflection of the primary beam only occurs at very small angles and does not cause any difficulties to the data acquisition process. In optical CT-based gel dosimetry, the bending of the visible light rays resulting from the refractive index change at the boundaries of the scanned dosimeters presents certain challenges. As is schematically shown in figure 3a, when the central region of a cylindrical dosimeter is optically scanned, a straight line passage of the incident light ray across the dosimeter can be obtained. When the incident laser beam is in the peripheral region, deviation from straight line passage is expected because of the multiple reflection and refraction around the boundary of the dosimeter. This phenomenon is more pronounced for dosimeters with containers of different refractive, and with increasing thickness of the containers (Gore et al, 1996).
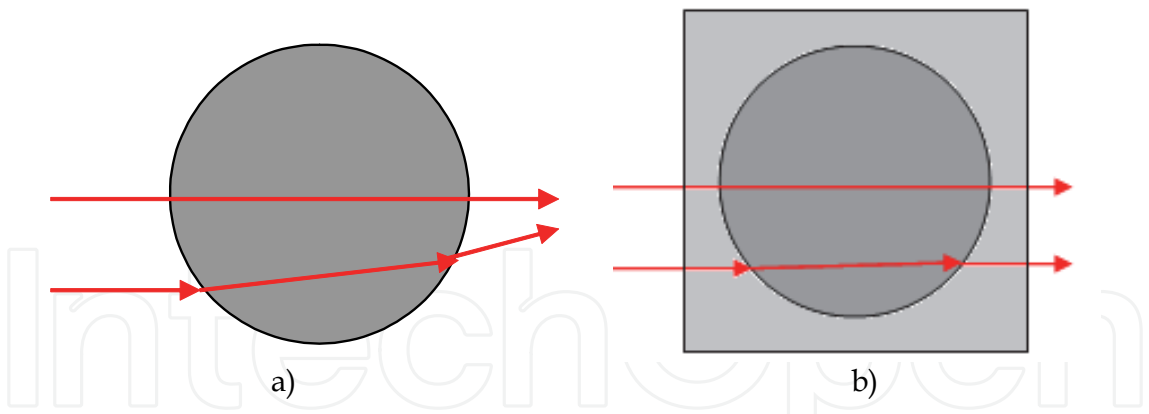
Fig. 3. Illustration of the laser path problem in optical CT: a) bending of the laser path because of the refraction at the surface of the cylindrical dosimeter; b) the use of refractive index matching liquid to maintain straight line laser passage.

The spatial and angular deflections of the light rays at the boundaries of the scanned dosimeters could cause practical difficulties to the data acquisition in optical CT. For scanners using a small area detector whose position is fixed relative to the scanning mirror, missing of the primary signal is possible depending on the degree of the deviation of the laser beam (Gore et al, 1996; Kelly et al, 1998; Xu et al, 2004). For scanners using a broad beam and a large area detector, the deflection could cause all or part of the optical density drop from a specific laser path to be wrongly assigned (Doran 2009).

One solution to this problem is to immerse the scanned dosimeter into a refractive index matching liquid during optical CT scanning (see figure 3b). The refractive matching liquid is normally housed in a rectangular tank with transparent walls. Computer simulation can be used to determine the optimal refractive index of the matching liquid for the diameter of the imaged dosimeter, the thickness of the container wall and the refractive indices of these two materials.

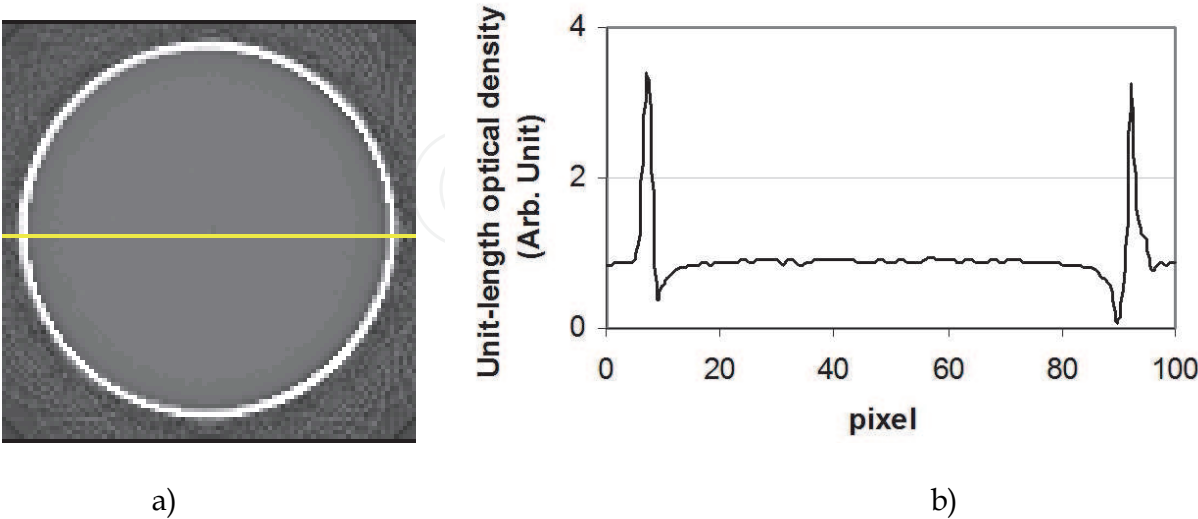a)   b)

Fig. 4. Results from scanning a BANG gel cylinder filled with non-irradiated gel using an OCT-OPUS™ optical CT scanner: a) reconstructed image of a transverse slice; b) line profile along the line shown in a).

Ideally, a perfect match would eliminate the effect of beam deflection completely and permit acquisition of data over the whole diameter of a dosimeter. In practice, it is not an easy task to make a matching liquid with the exact refractive index from calculation. Furthermore, the reflection of the beam at the interface can not be eliminated simultaneously. Figure 4 shows a line profile on a reconstructed transverse slice of an un-irradiated BANG gel phantom (Barex container with 17 cm diameter and 1 mm thickness) from the OCTOPUS™ optical CT scanner (Xu et al, 2004). When the laser beam hits the container wall from outside, part of the beam is reflected and deflected from the forward direction. This causes a sudden drop in the signal. As the laser beam moves further, more light gets transmitted and collected, but the structure of the signal becomes complicated by the multiple refraction and reflections along the container wall. It is only when the laser is sufficiently far away (about 2cm) from the inner side of the container wall that the signal flattens out to within 3 to 4%.

The effect of light reflection and refraction on optical-CT based 3D dosimetry is at least twofold: first, most of the dosimetric phantoms have been made as cylinders so far, to make the effect of multiple refraction and reflection easy to model. Second, the useable region of a dosimeter is usually limited, excluding a region that is a few millimeters or a few centimeters from the surface of the dosimeter.

4. Dynamic ranges of optical CT scanners

The dynamic range of an optical CT scanner is an important factor in the designing and operation of optical CT-based 3D dose verification systems. As an irradiated gel dosimeter is optically scanned in three dimensions, the net optical density function usually changes in a much wider range than it does in 2D study of the same plan using film dosimeters. This phenomenon is caused by the longer and varying path lengths of the laser beams associated with 3D CT scan. Therefore, development of methods for adjusting gel formation and reducing noise level in optical CT scanner is necessary for optimal image contrast.

The usable dynamic range of a scanner is usually limited by several aspects of the configuration of the scanner, including the noise level in the signals collected and the performance of the image reconstruction algorithm that processes the signals. For instance, a scanner with a 16-bit A/D data acquisition board has a fundamental digitization noise of 2^{-16}, thereby limiting the dynamic range of the scanner to less than 4.8 (Xu et al, 2003). The effective dynamic range of the scanner is further narrowed by the signal-to-noise requirement and the electronic and mechanic noises in the scanner. Therefore, when such scanners are used for 3D dose verification, cautions should be taken to ensure that the optical density increments along all possible paths during scanning of an irradiated gel never exceed a certain maximum. On the other hand, the maximum optical density increment across an irradiated gel is desired to be as close to the effective dynamic range of the scanner as possible, in order to maintain high signal-to-noise ratio and thus high dosimetric accuracy.

Figure 5 demonstrates the effect of over-dosing by comparing the reconstructed images for transverse slices with maximum optical density increments of 2.5, 2.8 and 3. The images were obtained from a BANG gel phantom irradiated with a 6MV, 6 cm x 6 cm square field using an OCTOPUS™ optical CT scanner with an effective dynamic range of 2.5 (Xu et al 2003). The depths of the transverse slices are 6 cm, 4 cm and 3 cm from the bottom of the dosimeter respectively). As can be seen from figure 5 (b) and (c), when the optical density increment (ODI) is larger than 2.5, an artifact arises in addition to the expected large

uncertainty and becomes more pronounced with increasing ODI. The dark stripes along the diagonal of the squares indicate that the signals in these regions were larger than their actual values. Also, the reconstruction artifact in these regions will be systematically propagated across the entire image as seen in Figure 5(c).
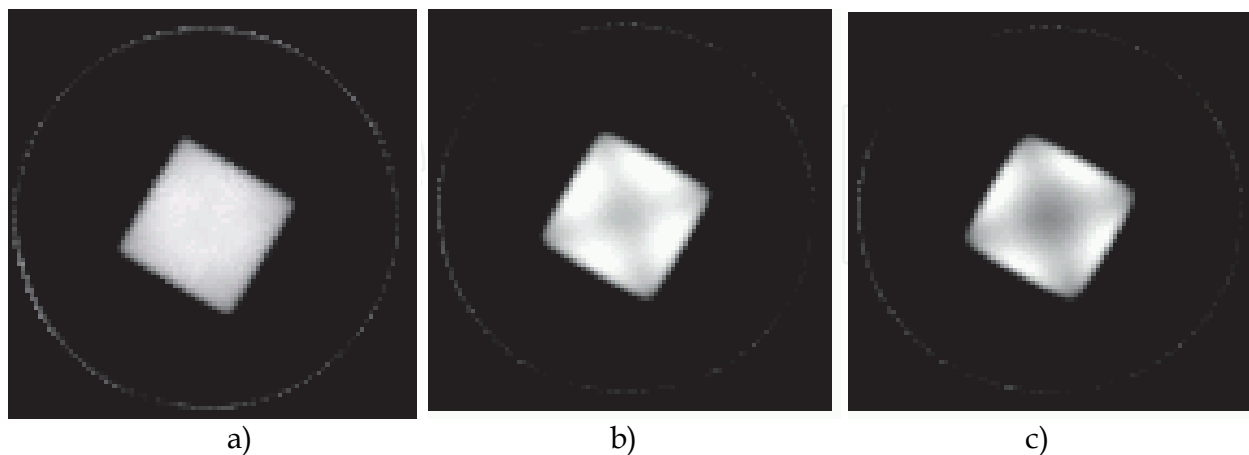

| a) | b) | c) |

Fig. 5. Reconstructed image for 3 transverse slices (depth 6, 4, 3cm) of a 6MV, 6cm x 6cm single field using an optical CT scanner of 2.5 dynamic range; the maximum optical density increments for these planes are 2.48, 2.8 and 3.1 respectively.

The distortions of the images in figure 5 (b) and 5(c) can be attributed primarily to the significant contribution from scattered photons at high ODI. In polymer gels, optical attenuation is caused by the Rayleigh/Mie scattering of light on polymer particles. Therefore, collection of some of the scattered photons at the detector's aperture is inevitable but normally does not cause any detectable error in the reconstructed image. With increasing optical density increments, the number of scattered photons produced increases whereas the intensity of the transmitted primary beam decreases. The fraction of the scattered light in the signals collected will increase and eventually become a significant source of error. The image reconstruction algorithm interprets the overestimated signals as less attenuation near the diagonals of the square field and produce less dose in these regions.

The optical density increments across an irradiated polymer gel depend on the dose response property of the gel material and the dose distribution delivered to the gel. To meet the requirement of the effective dynamic range of a scanner, it is necessary to predict theoretically the maximum optical density increment across an irradiated polymer gel first before actual dose delivery and optical scanning. Adjustment to gel formulation can be made in advance to get optimal scanning results.

The optical density for a given path s across an irradiated gel is the line integral of the unit-length optical density function along the path:

$$OD(s) = \int (A_0 + kD(r)))dr \qquad (1)$$

where A_0 is a constant characterizing the unit length opacity of the non-irradiated gel, k is the slope of the calibration function (or gel sensitivity), and $D(r)$ is the dose at point r. The sensitivity k of BANG® gels can be chemically modified by the manufacturer. The net optical density increment (*ODI*) along the path s across the irradiated gel is:

$$ODI = \int A(r)dr - A_0\int dr = k\int D(r)dr \qquad (2)$$

since the maximum ODI_{max} across an irradiated gel is constrained by the usable dynamic range of the scanner, the optimal sensitivity factor k for study of a treatment plan can be determined by finding the maximum value $max\{\int D(r)dr\}$ from among all line integrals of dose across all projections in all axial slices of the dose distribution to be delivered. The sensitivity factor can then be determined from:

$$k = ODI_{max} \Big/ max\{\int D(r)dr\} \qquad (3)$$

Figure 6a shows a schematic picture of the computer program for the calculation of the maximum optical density increment on the plane of optical CT scanning. The dotted line in Figure 6b is the laser path with maximum optical density increment for a transverse slice of an IMRT plan. The maximum optical density increment during the process of scanning a gel phantom can be obtained by comparing all the maximum values on different transverse slices.

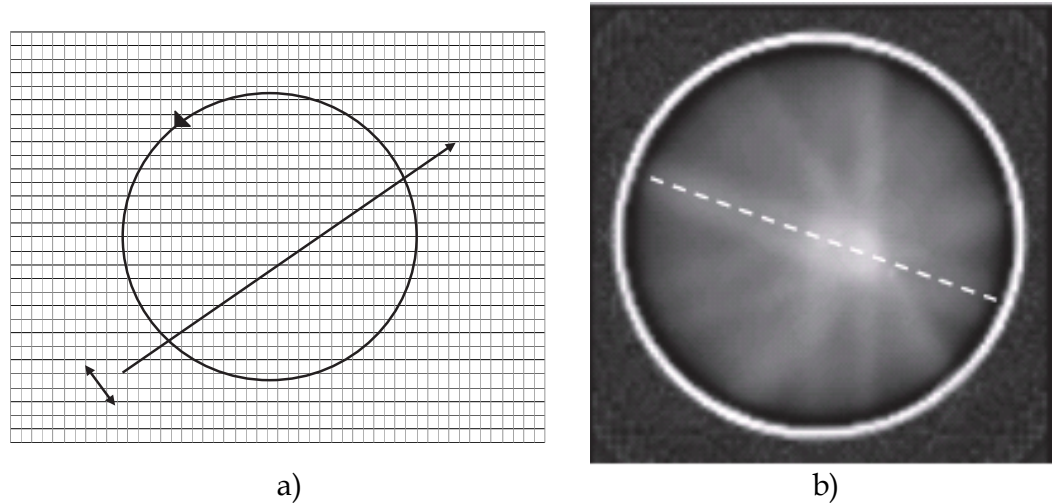a)   b)

Fig. 6. a) schematic picture for calculation of the maximum optical density increment in the plane of scanning: circle, boundary of the gel container and the integration region; little square, pixel; long arrow, laser beam. The computer program simulates the translation of the laser beam and the rotation of the container as indicated by the short arrows; b) a transverse slice of a 5-field IMRT irradiation; the white dashed line indicates the laser path with maximum optical density increment for the slice.

5. Light scattering in optical CT

Light scattering is also an important concern in optical CT-based gel dosimetry. In theory, only the portion of the incoming laser beam that survives the multiple Rayleigh-Mie scattering and/or light absorption in the forward direction should be used for image reconstruction. But collection of scattered photons in the detector apertures is inevitable in all optical CT scanners. Artifacts caused by the scattered light in optical CT could be more difficult to deal with than those in conventional X-ray CT considering the high penetrating power of X-ray beams (Olding et al, 2010).

To quantitatively estimate the intensity of the scattered light in regions where light signals might be collected for image reconstruction in optical CT-based 3D dosimetry, a Thorlabs PM100D optical power meter (Thorlabs Inc, Newton, NJ, USA) with an optical sensor of 1 mm diameter sensitive area was used (Xu et al, 2010b). The dosimetry phantom to be measured was put into the scanning tank of an OCTOPUS™ optical CT scanner (MGS Research Inc, Madison, CT, USA) filled with a refractive index matching liquid. A laser diode was positioned at one side of the water tank to generate a stationary laser beam of 0.8 mm width. On the other side of the tank, an in-house manufactured positioning system was used to move the optical sensor in the direction perpendicular to the outgoing laser beam from the dosimeters at an increment of 1 mm.

To compare the light scattering effect in different types of dosimeters, a BANG gel phantom and a Presage phantom were made as cylinders of 15.2 cm diameter and 10 cm height. Both dosimeters were irradiated with 6 MV photons using a Varian Clinac 2100EX. The irradiations were given such that the maximum optical density drops across the dosimeters are close to the dynamic range of the OCTOPUS™ optical CT scanner (about 2.5).

Figure 7 plots the relative intensities of the scattered light as a function of the off-axis distance for the matching liquid only and for those with a dosimeter in place. The relative intensities are normalized to the intensities of the primary beam at the center position (about 1500 milli-watts, 5 milli-watts and 5 milli-watts respectively). The intensities of the scattered light from both dosimeters were found to be more than 1% of the primary light signal within 2 mm from the laser beam but decreases sharply with increasing off-axis distance. The amount of scattered photons from the Presage dosimeter is more than an order of magnitude larger than that from the same position of the refractive index matching liquid. The amount of scattered photons from the BANG gel dosimeter is approximately an order of magnitude larger than that from the Presage dosimeter.
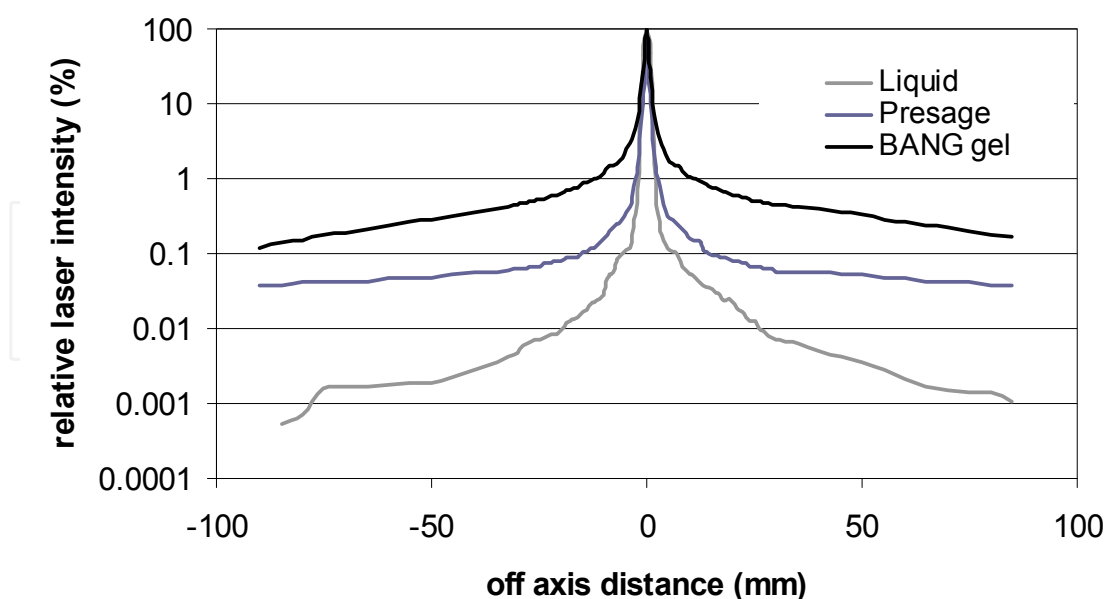

Fig. 7. Comparison of the scattered light intensity distributions from the BANG gel dosimeter, the Presage dosimeter and the matching liquid. Both dosimeters were irradiated to have a maximum optical density drop of 2.5.

The result shown in figure 7 is consistent with the fact that BANG gel is a scattering media and Presage is an absorbing media (Baldock et al, 2010). In theory, artifacts caused by the scattered light in optical CT scanners using a single laser source can be eliminated by reducing the detector apertures. In CCD-based optical CT scanners, telecentric lens can be used to select parallel beams from the scanned dosimeters (Krstajic and Doran, 2006; Sakhalkar and Oldham, 2008), thus minimizing the collection of the scattered light in the camera apertures.

6. Results

The ultimate goal of optical CT-based gel dosimetry is to verify radiation dose distribution in 3D. The major challenge in gel dosimetry is to achieve a spatial and dose accuracy and precision that satisfy the requirements for 3D dose verification of radiation treatments that are performed in the radiation hospital. Extensive study has been done on the development of a fast, accurate optical CT scanner and a stable gel manufacture system. A clinically applicable 3D dose verification system is not available at present time but results obtained so far are promising.
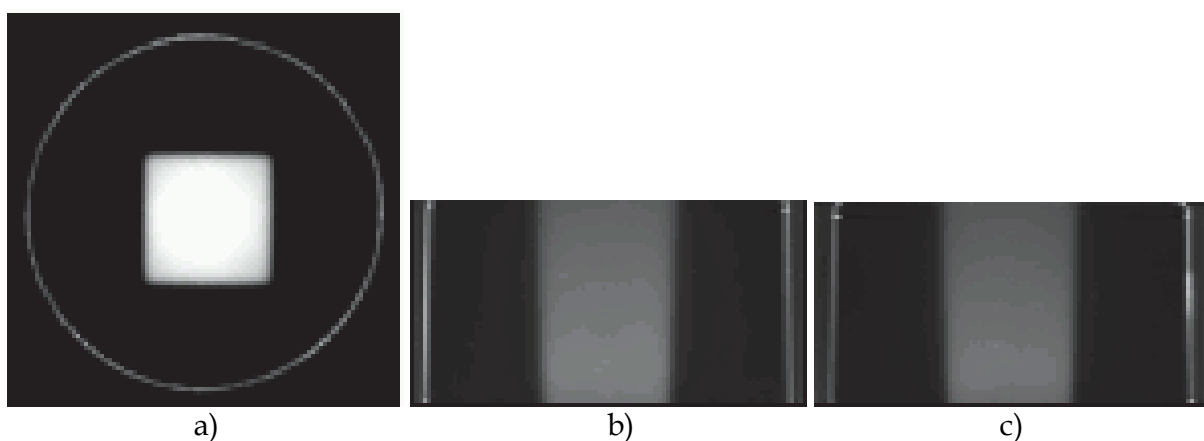
Fig. 8. Reconstructed images from scanning a cylindrical BANG gel phantom irradiated with a 6cm x 6cm, 6MV single field: a) transverse slice at 8cm depth; b) coronal slice passing through the central axis; c) sagittal slice passing through the central axis.

Figure 8 shows the grayscale images for one slice in each direction from scanning a cylindrical BANG gel phantom irradiated with a 6 cm x 6 cm, 6MV radiation field (Xu et al, 2004). The coronal and sagittal images were obtained by re-slicing the reconstructed transverse slices from optical CT using the ImageJ software. The positions of the container wall and the main features of the square field are reproduced well in these images.

Figure 9 compares the absolute dose distributions from the gel measurement and the Eclipse planning system for one transverse and one coronal slice of a BANG gel phantom irradiated with a 6 cm x 6 cm, 12 MeV electron field. The 3-D gel dose distributions were obtained using the dose response curve extracted from the percent depth dose curve of a 16 MeV, 6 cm x 6 cm single field irradiation (Xu et al, 2010a). The BANG gel phantoms used in this study were 17 cm diameter x 12 cm high cylinders thermoformed from 1 mm-thick Barex plastic sheet. The irradiated gel phantoms were scanned using an OCTOPUS™ optical CT scanner. The scans were done with 1 mm pixel size, 200 pixels per projection, 300 projections

per slice (for a total rotation angle of 180) and a slice separation of 1 mm. The slice thickness was about 0.6 mm (diameter of the laser beam). The phantoms were scanned within 4 days after the irradiations, with a scanning time of about 10 hours for each phantom (100 slices). All the features of the planned dose distributions were well reproduced in the gel experiment.
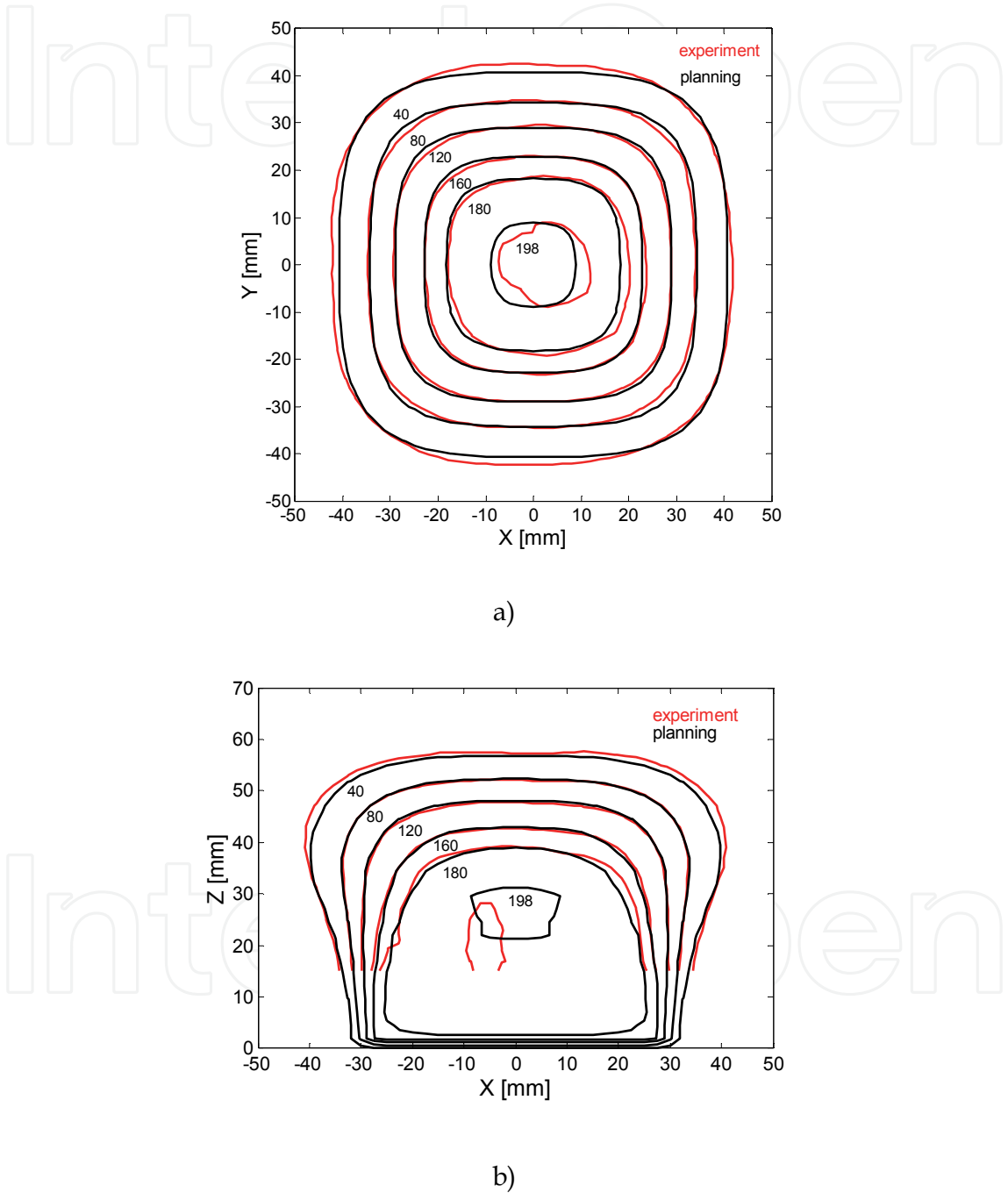

a)

b)

Fig. 9. Comparison of the isodose lines (198, 180, 160, 120, 80 and 40 cGy) from the gel measurement (red lines) and the treatment plan (black lines) for a 12 MeV, 6 cm x 6 cm electron field: a) transverse slice at 3.5 cm depth; b) coronal slice that passes through the isocenter.
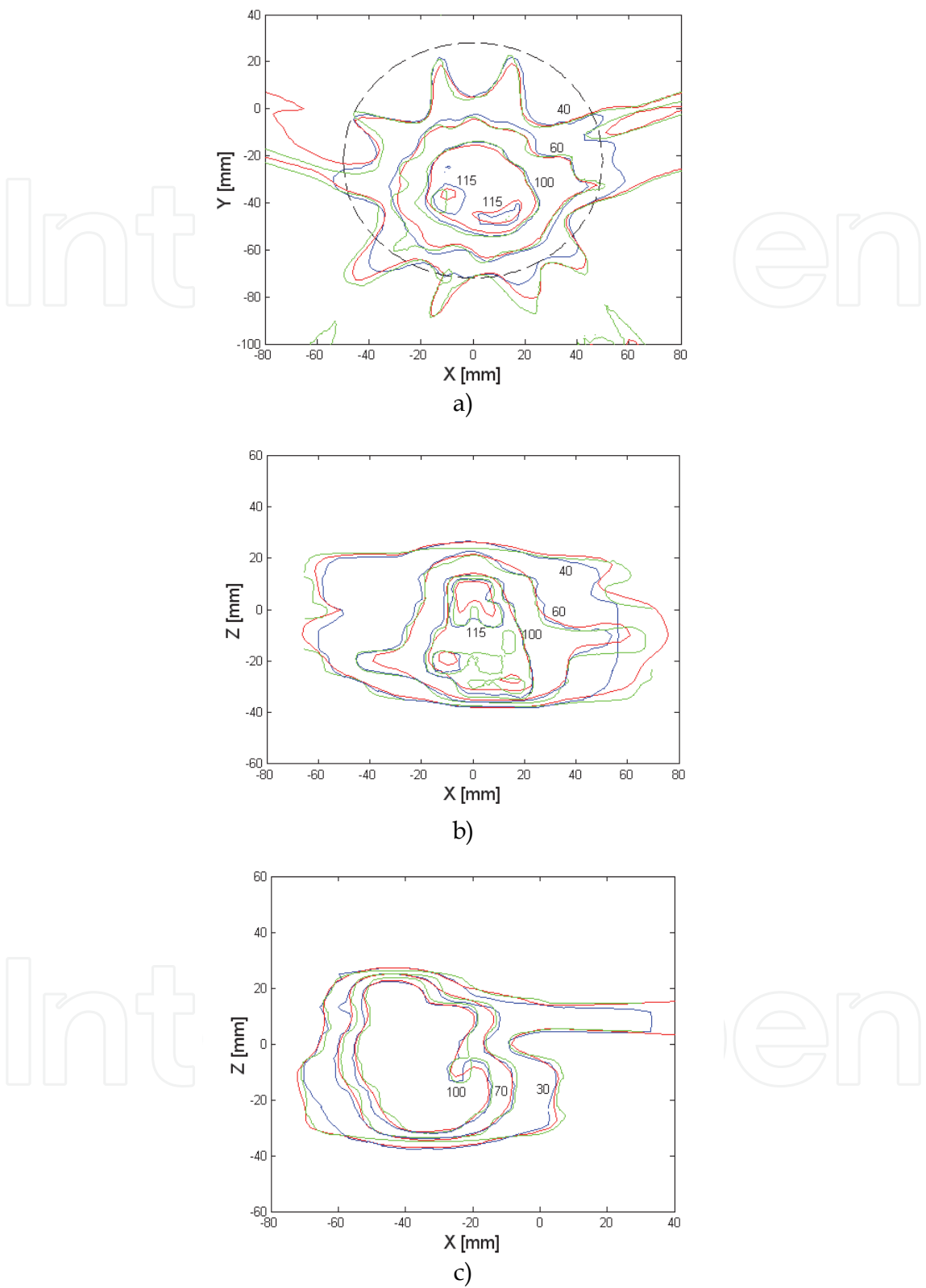
Fig. 10. Comparison of isodose dose distributions from treatment planning calculations (red), gel measurement (blue), and EDR2 measurements (green) for a 5 field IMRT plan: a) transverse slice; b) coronal slice; c) sagittal slice. All slices passes through the isocenter.

Figure 10 shows comparison of the isodose dose distributions from the gel measurement (blue lines), the film measurement (green lines) and the Eclipse-Helios treatment planning system (red lines) for a 5 field IMRT irradiation (Wuu and Xu, 2006). The IMRT plan used in this study was a real treatment plan for a patient with a small brain tumor (19.8 cc) generated by the Helios inverse planning system (Varian Corporation, Palo Alto, CA, USA). The plan delivered 180 cGy to the 100% isodose, with maximum dose around 218 cGy. The leaf sequence files and monitor units for the patient plan were used to generate a hybrid phantom plan, which was delivered in a 24x24x20 cm phantom. This phantom geometry was used for gel and film measurements. For comparative dosimetry the cylindrical gel phantom was immersed in a 24x24x20 cm water tank during IMRT irradiation. The gel phantom used was also a BANG gel cylinder with 17 cm diameter and 12 cm height. The gel irradiation was performed under the same set-up geometry as used in the hybrid phantom plan. The set-up geometry of the gel measurement was verified with the source-to-surface distance from irradiation.

The irradiated gel phantom was scanned using an OCTOPUS™ optical CT scanner (MGS Research, Inc., Madison, CT, USA) with 1 mm resolution. The reconstructed transverse images were normalize to two selected points of the treatment plan along the central axis, one at 98% dose and the other at 70% dose, to obtain the 3D relative dose distribution inside the irradiated gel. The results show good agreement among all three methods in all the three directions. The dose distribution in the axial direction from gel measurement is valid only in the regions marked by the dotted circle. The limited useful volume (in the central region with 75% of the diameter of the gel container) in the gel is due to the erroneous optical density values caused by the reflection and refraction of the laser rays at the interface between the gel and the container (Xu et al, 2004). This study demonstrates the feasibility of using a gel phantom to perform 3D dose verification of a complex radiation treatment plan.

7. Conclusions

Optical CT-based gel dosimetry is a promising technique that could have wide applications in radiation therapy physics. Extensive studies have been done on the development of different types of gel formulas, implementation of various optical CT scanners for gel dosimetry, and technical advantages and difficulties associated with 3-D dosimetry. The framework for optical CT-based 3D dosimetry is well established. The properties of the BANG gel polymer dosimeter and the Presage dosimeter have been intensively studied. The speed and the accuracy of the optical CT scanning process have improved significantly over the past 15 year. In particular, scanners with broad beam illustrations have been designed based on both parallel beam and cone beam geometry. Three dimensional dose measurements have been performed on various radiation treatment delivery units and compared with those from treatment planning systems and other dose measurement tools. The 3D gel dosimetry has been demonstrated to be comparable to the existing dose measurement tools in terms of dosimetric accuracy and spatial resolution. The challenge remained is to develop a fast, accurate, and robust 3D dose verification system that satisfies the requirements from routine clinical practice of radiation therapy physics. Development of software tools for the display and the quantitative evaluation of 3D dose distributions is also an area to explore.

8. References

Adamovics, J. & Maryanski, M. J. (2006). Characterization of PRESAGE: a new 3-D radiochromic solid polymer dosimeter for ionizing radiation *Radiat. Prot. Dosim.* 120 107–12

Audet, C. & Schreiner, L. J. (1997). Multiple-site fast exchange model for spin-lattice relaxation in the Fricke-gelatin dosimeter *Med. Phys.* 24 201-209

Baldock, C., Burford, R. P., Billingham, N., Wagner, G. S., Patval, S., Badawi, R. D. & Keevil, S. F. 1998 Experimental procedure for the manufacture and calibration of polyacrylamide gel (PAG) for magnetic resonance imaging (MRI) radiation dosimetry *Phys. Med. Biol.* 43 695–702

Baldock, C., De Deene, Y., Doran, S., Ibbott, G., Jirasek, A., Lepage, M., McAuley, K. B., Oldham, M., & Schreiner, L. J. (2010). Polymer gel dosimetry *Phys. Med. Biol.* 55 R1-R63

De Deene, Y., De Wagter, C., Van Duyse, B., Derycke, S., De Neve, W. & Achten, E. (1998). Three dimensional dosimetry using polymer gel and magnetic resonance imaging applied to the verification of conformal radiation therapy in head and neck cancer *Radiol. Oncol.* 48 283-291

DeJean, P., Senden, R., McAuley, K. B., Rogers, M. & Schreiner, L. J. (2006). Initial experience with a commercial cone beam optical CT unit for polymer gel dosimetry II: Clinical potential *J. Phys. Conf. Ser.* 56 183–186

Doran, S. J., Koerkamp, K. K., Bero, M. A., Jenneson, P., Morton, E. J. & Gilboy, W. B. (2001). A CCD-based optical CT scanner for high-resolution 3D imaging of radiation dose distributions: equipment specifications, optical simulations and preliminary results *Phys. Med. Biol.* 46 3191-3213

Doran, S. J., Nowais, S., Krstajic, N., Adamovics, J., Kacperek, A. & Brunt, J. (2006). True-3D scans using PRESAGE™ and Optical-CT: A case study in proton therapy *J. Phys. Conf. Ser.* 56 231–234

Doran, S. J. (2009). The history and principles of optical computed tomography for scanning 3-D radiation dosimeters: 2008 update *J. Phys. Conf. Ser.* 164 012020

Fong, P. M., Keil, D. C., Does, M. D. & Gore, J. C. (2001). Polymer gels for magnetic resonance imaging of radiation dose distributions at normal room atmosphere *Phys. Med. Biol.* 46 3105–13

Gore, J. C., Kang, Y. S. & Schulz, R. J. (1984). Measurement of radiation dose distributions by nuclear magnetic resonance (NMR) imaging *Phys. Med. Biol.* 29 1189-97

Gore, J. C., Ranade, M., Maryanski, M. J. & Schulz, R. J. (1996). Radiation dose distributions in three dimensions from tomographic optical density scanning of polymer gels: I. Development of an optical scanner *Phys. Med. Biol.* 41 2695-2704

Hilts, M., Audet, C., Duzenli, C. & Jirasek, A. (2000). Polymer gel dosimetry using x-ray computer tomography: A feasibility study *Phys. Med. Biol.* 45 2559-2571

Islam, K. T. S., Dempsey, J. F., Ranade, M. K., Maryanski, M. J. & Low, D. A. (2003). Initial evaluation of commercial optical CT-based 3D gel dosimeter *Med. Phys.* 30 2159-2168

Kelly, R. G., Jordan, K. J. & Battista, J. J. (1998). Optical CT reconstruction of 3D dose distributions using the ferrous-benzoic-xylenol (FBX) gel dosimeter *Med. Phys.* 25 1741-50

Krstajic, N. & Doran, S. J. (2006). Focusing optics of a parallel beam CCD optical tomography apparatus for 3D radiation gel dosimetry *Phys. Med. Biol.* 51 2055-2075

Lepage, M., McMahon, K., Galloway, G. J., De Deene, Y., Back, S. A. & Baldock, C, (2002). Magnetization transfer imaging for polymer gel dosimetry *Phys. Med. Biol.* 47 1881-90

Lopatiuk-Tirpak, O., Langen, K. M., Meeks, S. L., Kupelian, P. A., Zeidan, O. A. & Maryanski, M. J. (2008). Performance evaluation of an improved optical computer tomography polymer gel dosimeter system for 3D dose verification of static and dynamic deliveries *Med. Phys.* 35 3847-3859

Low, D. A., Dempsey, J. F., Venkatesan, R., Mutic, S., Markman, J., MarkHaacke, E. & Purdy, J. A. (1999). Evaluation of polymer gels and MRI as a 3D dosimeter for intensity-modulated radiation therapy *Med. Phys.* 26 1542-51

Maryanski, M. J., Gore, J. C., Kennan, R. P. & Schulz, R. J. (1993). NMR relaxation enhancement in gels polymerized and cross-linked by ionizing radiation: a new approach to 3D dosimetry by MRI *Magn. Reson. Imaging* 11 253-258

Maryanski, M. J., Zastavker, Y. Z. & Gore, J. C. (1996). Radiation dose distributions in three dimensions from tomographic optical density scanning of polymer gels: II. Optical properties of the BANG polymer gel *Phys. Med. Biol.* 41 2705-2717

Mather, M. L. & Baldock, C. (2003). Ultrasound tomography imaging of radiation dose distributions in polymer gel dosimeters: Preliminary study *Med. Phys.* 30 2140-2148

Oldham, M., Siewerdsen, J. H., Shetty, A. S. & Jaffray, D. A. (2001). High resolution gel-dosimetry by optical-CT and MR scanning *Med. Phys.* 28 1436-1444

Oldham, M. & Kim, L. (2004). Optical-CT gel-dosimetry II: Optical artifacts and geometrical distortion *Med. Phys.* 31 1093-1104

Olding, T., Holmes, O. & Schreiner, L. J. (2010) Cone beam optical computed tomography for gel dosimetry I: scanner characterization *Phys. Med. Biol.* 55 2819-2840

Pappas, E., Maris, T. G., Angelopoulos, A., Paparigopoulou, M., Sakelliou, L., Sandilos, P., Voyiatzi, S. & Vlachos, L. (1999). A new polymer gel for magnetic resonance imaging (MRI) radiation dosimetry *Phys. Med. Biol.* 44 2677–84

Sakhalkar, S. & Oldham, M. (2008). High-resolution 3D dosimetry utilizing a novel optical-CT scanner incorporating tertiary telecentric collimation *Med. Phys.* 35 101-111

Webb, S. (2001). Verification of 3D Dose Distribution, in: *Intensity Modulated Radiation Therapy*, Institute of Physics Publishing, ISBN 0750306998, 2001.

Wolodzko, J. G., Marsden, C. & Appleby, A. (1999). CCD imaging for optical tomography of gel radiation dosimeters *Med. Phys.* 26 2508–13

Wuu, C. S., Schiff, P. B., Maryanski, M. J., Liu, T., Borzillary, S. & Weinberger, J. (2003). 3D dosimetry study of Re-188 liquid balloon for intravascular brachytherapy using bang polymer gel dosimeters *Med. Phys.* 30 132-137

Wuu, C. S., & Xu Y. (2006). Three-dimensional dose verification for intensity modulated radiation therapy using optical CT based polymer gel dosimetry *Med. Phys.* 33 1412-1419

Xu, Y., Wuu, C. S. & Maryanski, M. J. (2003). Determining optimal gel sensitivity in optical CT scanning of polymer gels *Med. Phys.* 30 2257-2263

Xu, Y., Wuu, C. S. & Maryanski, M. J. (2004). Performance of optical CT scanning of polymer gels as a tool for 3D dose verification *Med. Phys.* 31 3024-3030

Xu, Y., Wuu, C. S. & Maryanski, M. J. (2010a). Sensitivity calibration procedures in optical CT scanning of BANG polymer gel dosimeters *Med. Phys.* 37 861-868

Xu Y., Adamovics J., Cheeseborough J., Chao K. S. & Wuu C. S. (2010b). Light scattering in optical CT scanning of Presage dosimeters *Journal of Physics: Conference series* 250, 012063
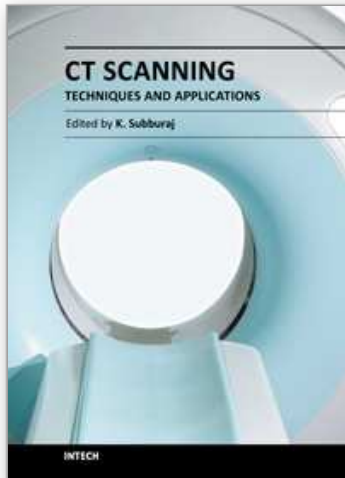
CT Scanning - Techniques and Applications

Edited by Dr. Karupppasamy Subburaj

Since its introduction in 1972, X-ray computed tomography (CT) has evolved into an essential diagnostic imaging tool for a continually increasing variety of clinical applications. The goal of this book was not simply to summarize currently available CT imaging techniques but also to provide clinical perspectives, advances in hybrid technologies, new applications other than medicine and an outlook on future developments. Major experts in this growing field contributed to this book, which is geared to radiologists, orthopedic surgeons, engineers, and clinical and basic researchers. We believe that CT scanning is an effective and essential tools in treatment planning, basic understanding of physiology, and and tackling the ever-increasing challenge of diagnosis in our society.

How to reference

In order to correctly reference this scholarly work, feel free to copy and paste the following:

INTECH

open science | open minds